COMMUNICATION

Check for updates

Stretchable and neuromorphic transistors for pain perception and sensitization emulation†

Yutong Xu,‡[a] Dapeng Liu,‡[a] Shilei Dai,[a] Junyao Zhang, [iD][a] Ziyi Guo,[a] Xu Liu,[a] Lize Xiong*[b] and Jia Huang [iD] *[ba]

Pain perception nociceptors (PPN), an important type of sensory neuron, are capable of sending out alarm signals when the human body is exposed to destructive stimuli. Simulating the human ability to perceive the external environment and spontaneously avoid injury is a critical function of neural sensing of artificial intelligence devices. The demand for developing artificial PPN has subsequently increased. However, due to the application scenarios of bionic electronic devices such as human skin, electronic prostheses, and robot bodies, where a certain degree of surface deformation constantly occurs, the ideal artificial PPN should have the stretchability to adapt to real scenarios. Here, an organic semiconductor nanofiber artificial pain perception nociceptor (NAPPN) based on a pre-stretching strategy is demonstrated to achieve key pain aspects such as threshold, sensitization, and desensitization. Remarkably, while stretching up to 50%, the synaptic behaviors and injury warning ability of NAPPN can be retained. To verify the wearability of the device, NAPPN was attached to a curved human finger joint, on which PPN behaviors were successfully mimicked. This provides a promising strategy for realizing neural sensing function on either deformed or mobile electronic devices.

New concepts

Pain perception nociceptors are a kind of nerve ending widely distributed in the peripheral tissues of the human body, which convey injury signals and maintain human safety. Enabling artificial intelligence devices with the neural sensing ability and building artificial sensory systems will be beneficial to diversify the functions of electronic devices as well as protect the safety of the devices. At the same time, the stretchability of neural sensor devices is key to the device availability when working on human skin or robotic joints. Here, we prepared fully stretchable artificial pain perception nociceptors and demonstrated the stable pain perception ability of the device in several scenarios such as planar stretching, curved surfaces, and human fingers.

Introduction

Sensation is a reflection of the individual characteristics of objective things that interact directly with the sensory organs and is received, integrated, and transmitted by the sensory nervous system (SNS), which is capable of innervating the various sensory tissues of the human body.[1,2] Noxious stimuli such as external excessive force, destructive temperature, adverse chemical stimuli, and intense light will cause pain. People always feel uncomfortable and tend to avoid such stimuli,[2,3] because excessive pain means causing damage to the body. As a special sensory neuron, the pain perception nociceptor (PPN) can send out pain signals when tissues are over-irritated and prevent the organism from further contact with harmful stimuli that cause damage to the body.[4] The ability of PPN to warn against excessive external stimuli is very important for human safety in daily life.

The human body gains rich perception through massive nerve endings, *i.e.*, receptors for various stimulus types, and can prevent overstimulation from causing injury, which has inspired the development of neural sensing of artificial intelligence devices. Bionic electronic perception units that can mimic the pain-sensing of organisms provide necessary functions in neural robots, electronic skins, and prostheses.[5,6] The bionic synapse, a structure that connects two adjacent neurons, is the basic unit for transmitting various physiological signals including pain sensation. Inspired by this, a great deal of work has been devoted to the development of artificial synaptic devices that are capable of mimicking biological neural functions and sensory systems. Based on the structural classification, artificial synapse devices can be mainly divided into three-terminal and two-terminal artificial synapse devices. As for the type of signal stimulation, artificial

[a] *School of Materials Science and Engineering, Tongji University, Shanghai 201804, P. R. China. E-mail: huangjia@tongji.edu.cn*

[b] *Translational Research Institute of Brain and Brain-Like Intelligence, Shanghai Key Laboratory of Anesthesiology and Brain Functional Modulation, Shanghai Fourth People's Hospital Affiliated to Tongji University, Tongji University, Shanghai, 200434, P. R. China. E-mail: lizexiong@tongji.edu.cn*

† Electronic supplementary information (ESI) available. See DOI: https://doi.org/10.1039/d3mh01766d

‡ These authors contributed equally to this work.

synaptic devices can be mainly classified into electronic synapses, photonic synapses, and optoelectronic synaptic devices.[7–11] As one of the classes of three-terminal devices, electrolyte-gated transistors can be used to construct artificial neurons, where ions in the electrolyte can migrate directionally when an electrical pulse is applied to the gate, regulating the channel current concurrently.[12–14] This process can be used to mimic the transmission of releasing neurotransmitters into the synaptic cleft after the presynaptic neuron reaches an action potential, which would trigger a change in postsynaptic neuron potential.[15–20] Researchers have simulated pain perception using ion-dielectric transistors, most of which consist of hard materials.[6,15,21–25] However, when the device is stuck to robots, electronic skin, or prostheses, functioning appropriately in sophisticated scenarios is necessary because deformations and stretching of skin and limbs frequently occur during the moving process.[16,26–30] Therefore, the preparation of stretchable bionic synaptic devices for pain sensing is of significance for many application scenarios of artificial intelligence devices, as well as manufacturing robots with "touch" and self-awareness of avoiding harm.[23]

In this work, we prepared stretchable electrolyte-gated synaptic transistors and successfully demonstrated key functions of PPN such as threshold, sensitization, and desensitization. The fully stretchable transistor displays similar synaptic behaviors at different strain ratios, including excitatory postsynaptic currents (EPSC) and paired-pulse facilitation (PPF). The stretchable transistor is designed in a fiber-shape channel, which is obtained by electrostatic spinning poly (3,3′′′-didodecyl quarter thiophene) (PQT-12) and poly (ethylene oxide) (PEO) mixing solution. The source–drain and gate nanowire electrodes are coplanar half-embedded in polydimethylsiloxane (PDMS) substrate, on which nanofibers are wrapped by the ionic dielectric. We showed that the device under 50% stretching has a pain perception property consistent with the unstretched state, demonstrating that under stretching our artificial PPN maintains its perception capabilities. Furthermore, the device was attached to a curved surface and human finger joints. Under finger-bending conditions, we obtained results similar to those of pain sensation simulation under planar stretching, indicating that our device can still maintain its ability to perceive external stimuli and warn against danger when it is placed on a dynamically deformed human and robotic body. Our development of a highly stretchable PPN transistor can strongly facilitate the flexible application of artificial sensory systems.

Results and discussion

PPN is a free nerve ending that exists in peripheral tissues of the human body. Unlike other types of receptors, PPN can respond to multiple forms of stimulation (temperature, pressure, or chemical stimulation) and transmit the location and intensity of the stimulus through the spinal cord to the central nervous system.[31] This helps people react promptly to prevent over-stimulation from causing injuries (Fig. 1(a)). The three key aspects of PPN are threshold, sensitization, and desensitization.[25,32–34]

The sensory neuron cell is a kind of pseudo-unipolar cell with two axon branches, one penetrating the peripheral tissues to receive sensory information while the other transmitting sensory information into the spinal cord and the cerebral cortex, where the subject perceives the dangerous situation and responds accordingly. PPN is crucial to the survival and health of an organism.[31,35] Giving artificial intelligence devices pain perception capabilities will greatly expand their application functions and self-protection capabilities. The successful emulation of PPN behaviors has paved the way for the creation of pain-sensitive neural devices that can conform to the human body/machine and adapt to various scenarios, thereby propelling the advancement of artificial intelligence neural sensing domains.

Based on a pre-stretching strategy, we prepared a fully stretchable ion-dielectric transistor with fiber channels, and the structure of the device is shown in Fig. 1(b). Fibers were prepared by electrospinning of a chlorobenzene–chloroform mixed solution of the poly (3,3′′′-didodecyl quarter thiophene) (PQT-12) and poly (ethylene oxide) (PEO). Fibers were transferred onto a 50% pre-stretched polydimethylsiloxane (PDMS) substrate with silver nanowire electrodes and released to obtain fiber-shaped channels that were naturally curvy in their relaxed state. Fibers only switched between flat and curved states in the stretching-releasing cycle. The electrical properties of the semiconductor fibers would not be affected (Fig. 1(c)). PEO was used as an auxiliary component to make the mixed solution spinnable.[36,37] Characterization showed that PQT-12/PEO nanofibers obtained by electrospinning had a uniform distribution of sulfur and carbon elements (Fig. S1(a)–(c), ESI†). Atomic force microscopy (AFM) showed that fiber diameters were between 600–700 nm (Fig. S1(d), ESI†). X-ray photoelectron spectroscopy (XPS) confirmed the existence of sulfur elements. The peak at the binding energy E_B = 164.06 eV corresponds to S2p$_{3/2}$ and the peak at the binding energy E_B = 165.28 eV corresponds to S2p$_{1/3}$ (Fig. S1(e), ESI†). The X-ray diffraction (XRD) pattern showed crystal diffraction peaks of PEO and PQT-12 (Fig. S1(f), ESI†). The diffraction peaks at 2θ = 19.2° and 23.2° belong to PEO. Among the diffraction peaks belonging to PQT-12, the peak at 2θ = 4.8° corresponds to the side chain interaction along the (100) plane and 2θ = 22° corresponds to the π–π orientation of the (010) plane. The diffraction peaks at 2θ = 11.2° along the (200) plane and 16.5° along the (300) plane represent the second and third-order reflection peaks respectively.[38]

Silver nanowires (AgNWs) half-embedded in PDMS were used as stretchable electrodes for our device. To further match the energy levels of organic semiconductor PQT-12, we exchanged the surficial silver of source–drain electrode nanowires for gold nanoparticles (AuNPs).[39,40] After the displacement reaction, nanowires embedded in PDMS elastomer remained smooth, while the external nanowires became rough and gold particles attached to AgNWs (Fig. 1(e)). The change in resistance of the electrode under stretching was negligible with or without replacement treatment (Fig. 1(f)). Diacryloyl poly (ethylene glycol) (PEDGA)/ionic liquid 1-ethyl-3-methylimidazolium bis (trifluoromethylsulfonyl) Imide ([EMIM]$^+$[TFSI]$^-$) composite ion gel was solidified

Fig. 1 (a) A schematic diagram of the biological pain-perception process. (b) Device structure diagram of PQT-12/PEO NAPPN. (c) Fabrication schematic diagram of the pre-stretching strategy for the fully stretchable device. (d) SEM images of the nanofibers on the PDMS substrate. (e) SEM image of AgNWs inside the substrate and AuNPs–AgNWs at the substrate surface. (f) Resistance of AgNWs and AuNPs–AgNW electrodes in the relaxed state, at 10%, 20%, 30%, 40%, and 50% strain. (g) Frequency-dependent capacitance of PEGDA/[EMIM] [TFSI] ion gel in the initial state and at 50% strain. (h) Optical photos of nanofibers in the relaxed state and at 50% strain.

using 2-hydroxy-2-methyl propiophenone (HOMPP, optical cross-linker) under a 365 nm UV laser as solid ionic electrolyte dielectric. The ion gel has a high dielectric constant, which allows the transistor to be regulated by the small gate voltage. High-content ionic liquid and high molecular weight polymer-carriers improve the stretchability of the gel. The capacitance can be maintained under stretching (Fig. 1(g) and Fig. S2, ESI†).[41] The directional migration and relaxation

of ions in the dielectric under the regulation of the gate voltage can simulate the movement of neurotransmitters in the synaptic cleft, which is a vital part of synaptic behavior in bio-synapses. The semiconductor fibers which are initially curvy only undergo morphological changes during stretching, and the channel length of the transistor remains unchanged during stretching. The path the carrier has to travel through is the same length, and the electrical

performance of semiconductor nanofibers remains stable during stretching. The resistance of the stretchable electrode and the capacitance of the stretchable solid electrolyte can be maintained under stretching. The above features provide the possibility for the realization of fully stretchable three-terminal artificial PPN devices. The optical photo of the flexible device and curvature change of nanofibers during stretching is shown in Fig. 1(h).

PPN is the essential sensory neuron that helps the human body avoid danger. Their function relies on the continuous transmission of sensory information to the brain *via* neuronal pathways. Synapses are the basic units to carry out the transmission task, as they mediate the information transfer and integration through synaptic plasticity.[25,33,42–48] Synapses consist of three parts: the presynaptic membrane, the synaptic cleft, and the postsynaptic membrane. The presynaptic membrane releases certain neurotransmitters that diffuse through the synaptic gap to the postsynaptic membrane, causing excitatory or inhibitory potentials in the postganglionic neurons (Fig. 2(a)).[49–53] In the simulation of bio-synaptic function, the voltage pulses applied to the gate can be regarded as spike potentials generated by excited pre-neurons, and the change of the channel conductance corresponds to the connection strength between two synapses.

The PQT-12/PEO nanofiber stretchable ion-dielectric transistor showed a three-order-of-magnitude change in source–drain current under low gate voltage modulation (1 V to −1.5 V) (Fig. 2(b)). Notably, due to the pre-stretching strategy, the

semiconductor fiber channel was slack and curvy in the initial state, and its electrical properties and aspect ratio remained unchanged under the stretching state. The transfer curves of devices hardly change at different stretching ratios (0%, 30%, 50%), with negligible changes in off-state and open-state current and threshold voltage (Fig. 2(b), (c) and Fig. S3, ESI†). The stretchable devices demonstrated basic synaptic behaviors such as excitatory postsynaptic current (EPSC) and paired-pulse facilitation (PPF) (Fig. 2(d) and (e)). When a negative pulse is applied to the transistor, $EMIM^+$ ions in the electrolyte are attracted to the coplanar silver nanowire gate side, while $TFSI^-$ ions move to the interface of the PQT-12-PEO fiber/electrolyte. Under the electrostatic coupling effect, the accumulated $TFSI^-$ ions increased the hole charge carriers in the conducting channel. After the removal of the gate voltage, the positive and negative ions distributed on both sides returned to the equilibrium state along the concentration gradient, and the channel current slowly recovered to the initial level.[54] This current-variation process is similar to the synaptic signal transmission. Fig. 2(d) depicts the EPSC behaviors triggered by a gate voltage (V_g) of −2 V under the initial state and 50% strain. To test the stretching durability and cycle variation of the device, the synaptic behavior of the device was tested after 100 50%-stretching cycles. As shown in Fig. S4 (ESI†), the switching ratio remained virtually unchanged and the EPSC of the device remained stable. Paired-pulse facilitation (PPF) happens when two presynaptic spikes arrive in succession, resulting in the EPSC caused by the later spike being greater

Fig. 2 (a) Structural schematic diagram of biological synapses. (b) Transfer characteristic of the stretchable PQT-12/PEO nanofiber transistor at 0%, 30%, and 50% strain. (c) The switching current of the stretchable transistor at different strain ratios (0%, 30%, and 50%). (d) EPSC induced by a pre-synaptic electronic pulse (−2 V, 100 ms) at the relaxed state (left) and 50% strain (right). (e) PPF behavior induced by a pair of pre-synaptic electronic pulses (−2 V, 10 ms) with an interval time of 10 ms in the relaxed state (left) and at 50% strain (right). (f) Comparison of the PPF index as a function of electric pulse interval (Δt) between two successive spikes (−2 V, 10 ms) when the device was in the relaxed state (blue) and at 50% strain (orange).

than that caused by the prior spike because of the synaptic plasticity. When two consecutive negative electrical pulses (−2 V for 10 ms with 10 ms interval) were applied to the gate of the device, the EPSC generated by the second pulse was larger than that by the first pulse, as shown in Fig. 2(e). The reason is that the ion-oriented distribution induced by the first pulse had not returned to the equilibrium state when the second pulse was applied. Thus, more ions would accumulate at the PQT-12-PEO fiber/electrolyte interface, resulting in a larger source–drain current of the device. This phenomenon is similar to the PPF behavior of biological synapses. When the device is stretched to 50%, the current enhancement of the device remains unchanged. The PPF index was then calculated to further explore the PPF performance of the synaptic device. The formula can be described as follows: PPF index = $A_2/A_1 \times 100\%$, where A_1 and A_2 are the excitatory current values generated by the first and second pulses, respectively. Fig. 2(f) compares the PPF index of the devices at the initial state and 50% strain, which can be well fitted by a double exponential function fit. The PPF index decreases with the increasing interval time between pulses, which is consistent with the biological behavior. In our work, the electrical signals last for milliseconds. As one of the key parameters for synaptic devices, the modulation speed of the conductance state of our device can be shortened by replacing electrolytes with higher ion mobility and shortening the ion diffusion distance. Generally, the smaller ions have higher mobility in their electrolyte. Besides, our co-planar electrodes could be optimized to the vertical structure. Placing the gate electrode on the top of the electrolyte would further shorten the migration distance of ions.[55–57]

PPNs are specialized receptors that could detect potentially damaging stimuli and protect the body by producing pain sensations and triggering defensive behavior.[58] Pain perceptual neurons are morphologically unspecialized free nerve endings widely distributed in the skin, muscles, joints, visceral organs, small vessels, and paracapillary connective tissue. The function mechanism of these sensory neurons is illustrated in Fig. 3(a). When a noxious stimulus is perceived at the peripheral end, neurotransmitters released from the anterior neuron bind to transient receptor potential (TRP) channels and G protein-coupled receptors (GPCRs) on the surface of the pain perceptual neurons.[35,59,60] Thus, the ionic permeability of the postsynaptic membrane in the pain perceptual neuron is altered, triggering an action potential.

For mild touch and appropriate temperature stimuli, PPN determines that the situation is safe, whereas strong force, excessive temperature, and harmful chemical stimuli trigger alertness. The intensity of the stimulus is one of the critical factors in determining whether the pain sensation is triggered.[23] A series of negative electronic pulses with different amplitudes (−0.5 V, −0.8 V, −1 V, −1.2 V, −1.5 V, −2 V, −3 V, 2 ms) were applied to the stretchable PQT-12/PEO NAPPN. As the electric pulse amplitude increased, more negative ions were attracted to the PQT-12-PEO fiber/electrolyte interface, and higher carriers were concentrated in the channel, thus the EPSC gradually increased (Fig. 3(b)).[61] When the electric pulse amplitude was lower than 2 V, the excitatory current could not

reach the threshold level (I_{th} = 10 μA) and no pain sensation would be generated. When the stimulus was stronger than 2 V, the device current would exceed the threshold. Here, we defined −2 V as the threshold voltage (V_{th}). Moreover, the greater damage inflicted on the organism, the longer it takes to recover to a healthy state.

Therefore, we studied the recovery process of the device current with different pulse amplitudes (Fig. S5a, ESI†). The larger EPSC takes a longer time to recover to the initial value, which is consistent with the biological behavior. Notably, the performances of stretched PQT-12/PEO NAPPN on pain sensation emulation and recovery time trend are consistent with those under the relaxed state (Fig. S5b, c and S6, ESI†). Recent works using electrolyte-gated transistors to simulate PPN and the threshold characteristics of their devices are shown in Table S1 (ESI†), and different from previous works, our devices are stretchable. Besides, our NAPPN exhibits a relatively shorter incubation time and higher response current in pain perception simulation, which means a faster response speed and higher sensitivity. The reason would be that the fiber-shaped channel was wrapped by ionic gel, which maximizes the semiconductor/electrolyte interface, thereby strengthening the modulation ability of the gate electrode. Furthermore, instead of using inorganic ions as active ions in relevant research work, the organic ions in our NAPPN not only have high capacitance but also good compatibility with organic field-effect transistors.[19] Weak stimuli may also cause injury under the conditions of contacting the organism for a long time, such as sunburn caused by prolonged exposure to the sun.[62] By applying a constant −1.5 V pulse (below V_{th}) to the device gate for a short time (2 ms), the EPSC did not reach the threshold and no pain was generated (Fig. 3(c)). When the duration was extended to 10 ms, the excitatory current exceeded the threshold level. The results suggest that the device successfully simulated the transition from non-pain to pain perception by prolonging the duration of external stimuli in biological pain receptors. The emulation of this behavior was successfully repeated on the device at 30% and 50% strain. The transition from non-painful cognition to painful cognition can also be achieved by applying repeated and frequent stimuli, which is known as "no-adaptation" behavior in biological PPN. This behavior is vital for protecting humans from repetitive low-intensity noxious stimuli.[21,63,64] This process can be mimicked by PQT-12/PEO NAPPN (Fig. 3(d)). A sequence of electrical pulses of different amplitudes (−0.9 V, −1.5 V, −2 V, −3 V) were applied as external stimuli. When the presynaptic spike decreased to a certain extent, the device current quickly saturated and never reached the threshold. However, once the amplitude increased to a certain magnitude (but below the V_{th}), the EPSC exceeded the threshold at a time point during the sequence period. The higher gate voltage drives more ions to move directionally. When the interval is too short (for example: 1 ms) for complete ionic relaxation, [TFSI]$^-$ ions at the PQT-12-PEO fiber/electrolyte interface gradually accumulate, which induces the enhancement of the device current. In contrast, the directional migration of ions caused by small pulses can completely return to the equilibrium state in such a short interval.
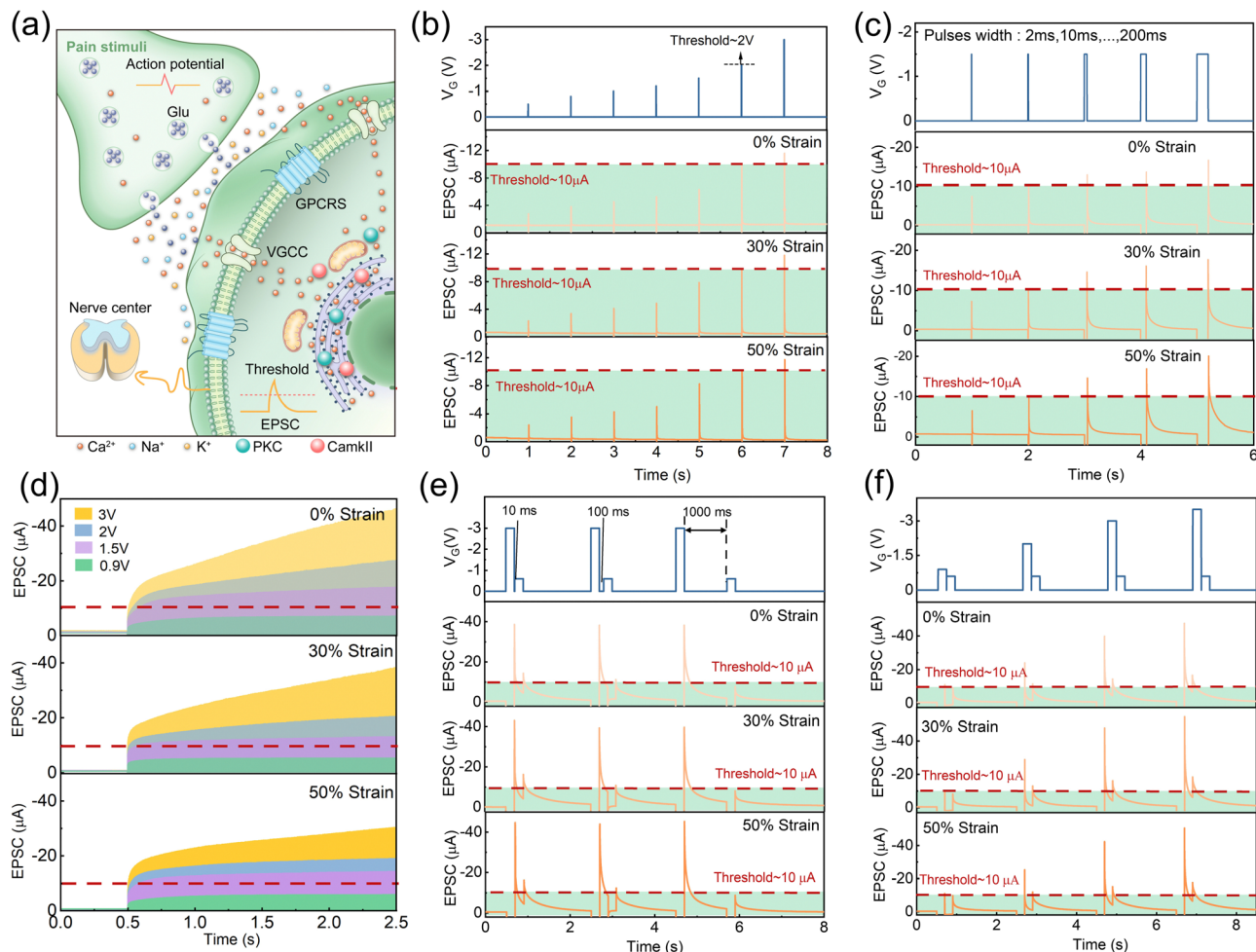
Fig. 3 (a) Working mechanism diagram of the pain-perceptual nociceptor. (b) The results of applying electronic pulses with various amplitudes (-0.5 V, -0.8 V, -1 V, -1.2 V, -1.5 V, -2 V, -3 V) to the gate for 2 ms, and the EPSC does not reach the threshold ($I_{th} = 10$ μA) until the amplitude reaches -2 V. (c) The results of applying electronic pulses (-1.5 V) to the gate for different time (2 ms, 10 ms, 50 ms, 100 ms, 200 ms), and the current does not reach the threshold until the duration is extended to 10 ms. (d) Mimicking the "no-adaptation" behavior by applying continuous multiple pulses (last for 2 ms for each pulse and interval for 1 ms) with different amplitudes (-0.9 V, -1.5 V, -2 V, -3 V). (e) Mimicking desensitization by applying a pair of electronic pulses (setting -3 V and -0.6 V as the pre and the post-pulse respectively, 200 ms) to the gate with different intervals (10 ms, 100 ms, 1000 ms). (f) Mimicking sensitization by applying pairs of electronic pulses (setting -0.6 V as the post pulse, 2 ms interval) with different pre-pulse amplitudes (-0.9 V, -2 V, -3 V, -3.5 V, 200 ms).

The two-phase sensitivity of temporal characteristics of PQT-12/PEO NAPPN at different strains was fit in Fig. S7 (ESI†).[65] In the simulation of "no-adaptation" behavior, the device current of 30% and 50% strain would become saturated more easily compared with the initial state. However, this feature does not affect the ability of PQT-12/PEO NAPPN to determine whether the EPSC triggered by the specific stimulus sequence exceeds the threshold current or not (Fig. 3(d)). In addition, as the amplitude of the pulse sequence increased, the incubation time for the device current to reach the threshold decreased, namely the pain can be generated by fewer pulses (Table S2, ESI†).

In addition to preventing harmful external stimuli from damaging the healthy body, PPN has a special threshold triggering mechanism to further protect the injured area.[42,62,66,67] This mechanism is called peripheral sensitization, which occurs when the pain caused by the first stimulus is pronounced and

manifested as allodynia and hyperalgesia phenomenon.[68] Allodynia is defined as increased sensitivity toward innocuous stimuli (such as light touch), which would lower the threshold triggering requirements. Hyperalgesia is defined as an enhanced response to painful stimuli (such as noxious mechanical force or heat).[15,34,35,69] Overall, peripheral sensitization provides injured tissues with higher alertness to detect potentially harmful stimuli and is an important neural response that assists in the healing of the body back to health.[2] The recovery time and stimulus intensity after the first injury are two important factors that would influence peripheral sensitization. The PQT-12/PEO NAPPN mimics this type of neural behavior (Fig. 3(e) and (f)).[34]

The effect of the time interval between pre- and post-injury on the peripheral sensitization of NAPPN was investigated. An electrical pulse (-3 V 200 ms) was applied as the first strong noxious stimulus, followed by a small electrical pulse (-0.6 V)

with the same duration as the second stimulus. The intervals between pre- and post-injury were set at 10 ms, 100 ms, and 1000 ms (Fig. 3(e)). It should be noted that the intensity and the duration of the second stimulus could not trigger the device current over the threshold alone, which can be considered harmless stimuli for undamaged tissues. Interestingly, when the time interval between two stimuli was short enough (*e.g.*, 10 ms), the triggered current by the second stimulus significantly exceeded the threshold. As the time interval becomes longer, the current generated by the second stimulus gradually decreases. When the time interval was extended to 1000 ms, the EPSC triggered by the second stimulus no longer exceeded the pain threshold. This phenomenon can be explained by the pulse interval affecting the relaxation migration of ions. When the interval is short enough, most migrated ions at the PQT-12-PEO fiber/electrolyte interface cannot return to the initial state before the second pulse arrives. The concentration of hole carriers in the conductive channel is higher than that caused by a single pulse. When the interval time is long enough, the residual effect of the first pulse is eliminated, which leads to the current induced by the two pulses becoming relatively independent.[54,61,70,71] This is consistent with the mechanism of self-protection in biology. To prevent unfavorable conditions for healing, damaged tissues become more sensitive to stimuli, to the extent that even stimuli that do not cause pain alone will be alerted by the body. If the body has sufficient time to recover to a healthy state, the tissue sensitivity will decrease. This process is called desensitization.[34,72] It is noteworthy that the PQT-12/PEO NAPPN at the initial state, 30% strain, and 50% strain showed fairly similar excitation currents and consistent desensitization behavior.

To further investigate the desensitization behavior of NAPPN affected by temporal factors, the sensitization degree

Z (sensitization degree) can be defined as the ratio of excitation current triggered by the first stimulus to that triggered by the second stimulus ($Z = A_1/A_2 \times 100\%$). An exponential equation based on the ion migration model is proposed to fit the correlation between sensitivity and recovery time,[25]

$$Z = K_0 e^{-\frac{\Delta t}{\tau}} + Z_0 \tag{1}$$

where Z_0 is the sensitization constant under steady state ($\Delta t \to \infty$), K_0 is the sensitization factor, and τ is the relaxation time constant of the sensitization behavior. Sensitization parameters of PQT-12/PEO NAPPN can be obtained by fitting curves (Fig. 4(a)–(d)). Under 0%, 30%, and 50% stretching, the relaxation constants were 231.79 ms, 184.10 ms, and 284.70 ms, respectively.[1] When the time interval is longer than the time constant, PQT-12/PEO NAPPN exhibits desensitization behavior.[25,34]

The sensitization behavior of PQT-12/PEO NAPPN affected by various stimulus intensities was also investigated. During the test, the amplitude of the first electric pulse was changed (−0.9 V, −2 V, −3 V, −3.5 V, 200 ms) while setting the stimulus interval (2 ms) and the second stimulus (−0.6 V 200 ms) as constants. When the first pulse was set at −0.9 V, the second pulse could not trigger the EPSC over the threshold, which means no bodily harm after these consecutive stimuli. When the first gate pulse gradually increased to −3.5 V, the output current triggered by the second pulse gradually increased and exceeded the threshold. The EPSC triggered by the second stimulus became larger as the intensity of the first pulse increased, which suggests that the first stimulus can influence the output current of the second stimulus at a certain interval. Namely, the current triggered by two pulses is not completely independent, in our test, 1 ms. A stronger pre-pulse drives
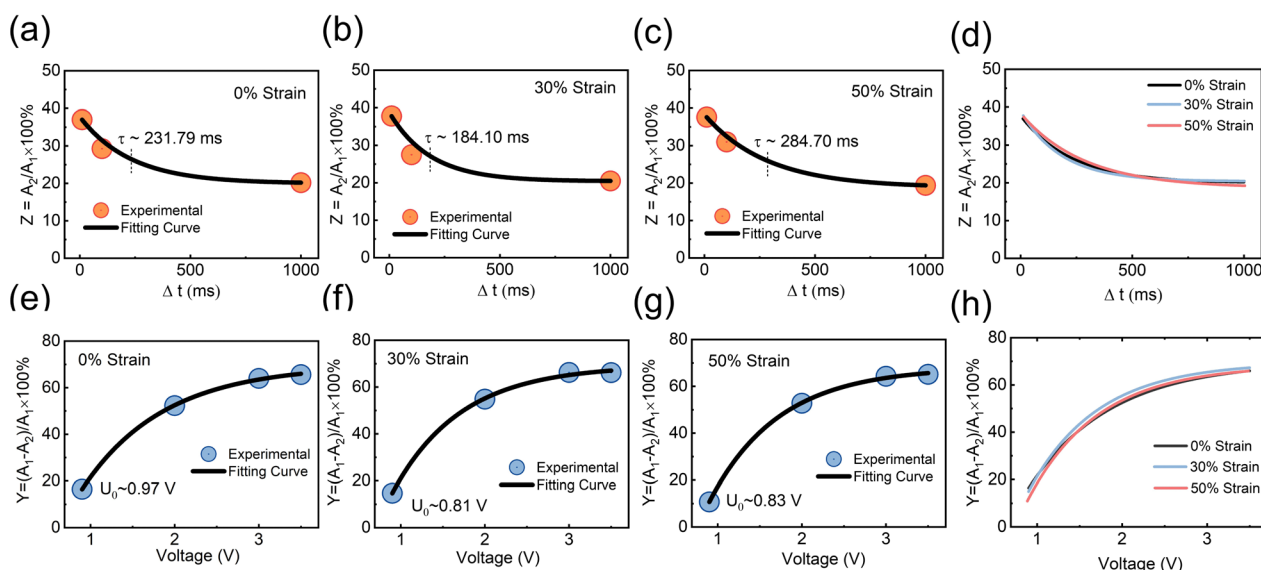

Fig. 4 The sensitization degree index (Z) of the fully stretchable NAPPN plotted as a function of the time interval (Δt) between two continuous stimuli at (a) 0%, (b) 30%, and (c) 50% strain. (d) Comparison of the fitting curve of the desensitization behavior of each stretching ratio. The degree of painful sensitization index (Y) of the fully stretchable NAPPN plotted as a function of the pulse amplitude of the first stimulus at (e) 0%, (f) 30%, and (g) 50% strain. (h) Comparison of the fitting curve of the sensitization behavior of each stretching ratio.

larger directional ion migration. At the same time interval, more unrelaxed ions aggregating at the interface lead to a higher EPSC after applying the post-pulse. This is consistent with the fact that severe biological injuries require more recovery time. Even low-intensity stimuli would cause hurt during the convalescence. Sensitization behavior can protect the body from exposure to stimuli that are not conducive to body healing in a short period after severe trauma.[73] Similarly, the device was stretched and tested under the same conditions. The results are consistent with the performance of the unstretched device, indicating that the device has a stable pain perception simulation ability. The degree of painful sensitization (Y) can be defined as $Y = (A_1 - A_2)/A_1 \times 100\%$, where A_1 and A_2 are the device current values triggered by the first stimulus and the second stimulus, respectively. We further investigated the interconnection between pain sensitization and stimulus intensity of the PQT-12/PEO NAPPN, which can be described by the following equation:[25]

$$Y = K_0 e^{-\frac{\Delta U}{U_0}} + Y_0 \qquad (2)$$

where K_0 and Y_0 denote two different sensitization constants, and U_0 is the characteristic voltage constant. When the first pulse is greater than U_0, sensitization behavior would occur. The characteristic voltage constants of the fully stretchable NAPPN under relaxed state, 30% strain, and 50% strain are 0.97 V, 0.81 V, and 0.83 V, respectively (Fig. 4(e)–(h)). Endowing artificial intelligence devices sensitized and desensitized pain perception properties could more comprehensively realize bionic perception functions and further protect device safety.

The fully flexible material system of the PQT-12/PEO NAPPN allows our device to attach tightly to a curved surface and mimic the characteristics of biological nociceptors (Fig. 5(a)–(d)). In Fig. 5(b), the current of the device is positively correlated with the amplitude and duration of the voltage applied to the gate. The result demonstrated the threshold characteristics of the PQT-12/PEO NAPPN, *i.e.*, external stimuli intensity and contact time are important factors affecting pain perception. As shown in Fig. 5(b), the EPSC increased with the enhancement of the applied
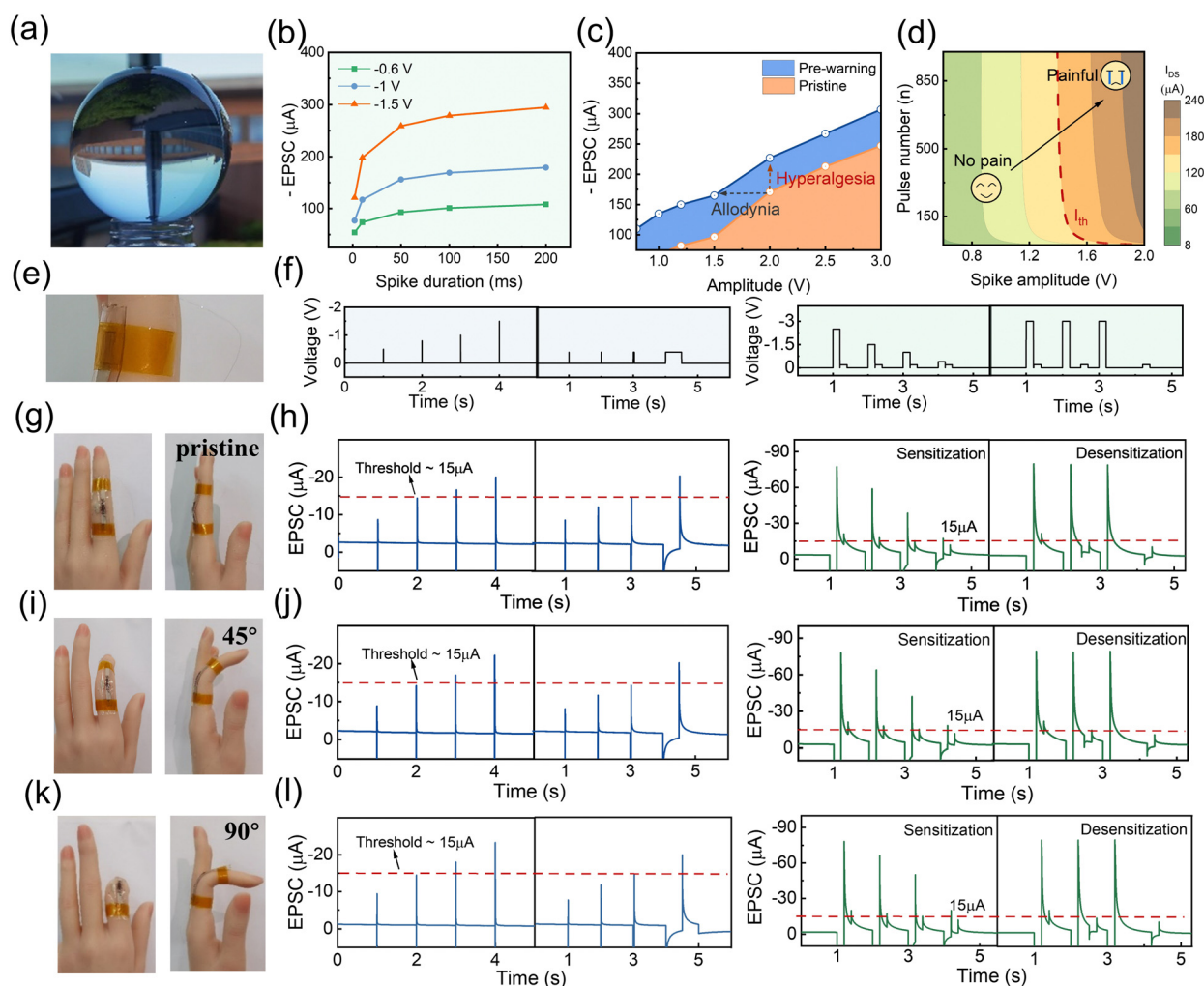

Fig. 5 (a) Optical photo of PQT-12/PEO NAPPN fitting tightly on a curved surface. (b)–(d) Key aspects of PPN mimicked by curved PQT-12/PEO NAPPN. (e) Wiring details for fully stretchable PPN wearable testing. (f) The sequence of electrical pulses applied to simulate the painful behavior of threshold, sensitization, and desensitization. The wearability and painful sensing performance of NAPPN while attached to (g) and (h) a natural straight finger, (i) and (j) a finger bent to 45°, and (k) and (l) a finger bent to 90°.

electrical signal. By applying a pre-pulse before the stimulation, the device on the curved surface was set into a pre-warning state (Fig. 5(c)). The PQT-12/PEO NAPPN in the pre-warning state will produce greater current values for the same intensity of the electrical pulse, *i.e.*, anomalous pain with nociceptive hypersensitivity symptoms. In addition, by adjusting the number and amplitude of external stimuli, the transition of PQT-12/PEO NAPPN from non-pain to pain perception can also be performed (Fig. 5(d)).

To confirm the promising flexibility of the PQT-12/PEO NAPPN required for practical applications such as electronic skin and human prostheses, the fully stretchable device was further attached to human finger joints for practical demonstration (Fig. 5(e)–(l)). The device was attached to a naturally straightened finger and then the finger joint was gradually bent to 90°, and the pain perception performance of NAPPN in response to electrical signals was then recorded. It is worth noting that, unlike planar stretching, during finger bending, the device has to cope with deformation and strain on the curved surface simultaneously. This is more similar to the scenarios in which biomimetic electronic devices were applied in real life. The characteristics of threshold, sensitization, and desensitization behaviors were simulated using the same test conditions, as shown in Fig. 5(f). The pain threshold was set at 15 μA, and our NAPPN demonstrated typical pain perception behavior when the finger is in a natural state (Fig. 5(g) and (h)). Subsequently, the synaptic behaviors of NAPPN to the same electrical stimulus at the bending angles of 45° and 90° were the same as those under the initial state (Fig. 5(i)–(l)). The above results suggest that the injury warning and pain perception ability of the NAPPN can be maintained under considerable surface deformation and stretching. Our work provides new strategies for designing artificial intelligence devices that can adhere to human skin, prosthetics, and robots with the ability of external-danger warning. The device can also maintain reliable performance under complex deformation conditions during limb movement. Neural sensing devices with this function will be able to avoid adverse injuries and ensure the safety of intelligent devices as well as users of the electronic prosthesis promptly.[74]

Conclusion

In conclusion, we prepared fully stretchable PQT-12/PEO nanofiber electrical synaptic devices with an electrostatic spinning technique. The devices exhibited typical synaptic behaviors such as EPSC and PPF under electrical pulse stimulation. When the device is stretched to 50%, the transistor properties and synaptic-like behaviors remain unchanged. At the same time, by simulating the external stimuli with electrical signals, PQT-12/PEO nanofiber synaptic devices successfully simulated the threshold, sensitization, and desensitization behaviors of biological PPN. Under 50% stretching, the pain perception ability is consistent with that under non-stretched conditions. Finally, we affixed fully stretchable NAPPN to human finger joints, and

the devices demonstrated consistent pain performance under considerable curvilinear deformation and strain caused by finger bending. Artificial intelligence devices with neural sensing and injury warning functions can efficiently prevent the device from prolonged exposure to destructive danger, which is meaningful for extending the life of devices. Highly flexible and stretchable devices are more similar to soft biological tissues in terms of deformation capability and can be applied in more complex scenarios other than flat surfaces. The fully stretchable PQT-12/PEO NAPPN prepared in this work provides a new implementation pathway for the preparation of flexible artificial intelligence sensor devices.

Experimental section

Electrospinning of single PQT-12/PEO nanofibers

PQT-12 (J&K, China) and PEO (M_W = 600 000 g mol^{-1}; Sigma–Aldrich) (w/w = 2 : 1) were mixed and stirred for 12 h in a cosolvent of chloroform/chlorobenzene (v/v = 1 : 1) to obtain a uniform solution (total concentration: 75 mg mL^{-1}). The solution was electrospun using a self-made electrospinning machine to obtain nanofibers (15 kV, the distance between the collector and the needle is 15 cm, and the injection speed is 0.1 mm min^{-1}).

Fabrication of NAPPN devices

Silver nanowires (10 mg mL^{-1}, ethanol solvent) were drop-casted on a clean glass substrate and heated at 60 °C for 30 min on a hot plate to evaporate the solvent. The substrate was then annealed at 200 °C for half an hour under a nitrogen atmosphere. Polydimethylsiloxane (PDMS) was mixed uniformly with a thermal crosslinking agent (w/w = 15 : 1) and drop-coated on the glass, then cured overnight in a 60 °C oven. The PDMS base embedding the silver nanowire electrode was cut into the desired shape and set aside. The PQT-12/PEO nanofibers were transferred to the pre-stretched PDMS base with both ends in contact with the source–drain electrode and slowly released. Diacryloyl poly(ethylene glycol)(PEGDA, M_W = 5000 g mol^{-1}), 2-hydroxy-2-methyl propiophenone (HOMPP), and 1-ethyl-3-methylimidazolium bis(trifluoromethylsulfonyl)imide ([EMIM]$^+$[TFSI]$^-$)(w/w = 1 : 0.2 : 5) were uniformly mixed and cured for 2 min under 365 nm ultraviolet light. The ion gel was cut into the desired shape and transferred onto the relaxed nanofibers to make it well in contact with the electrodes and semiconductor nanofibers.

Characterization

PQT-12/PEO nanofiber was observed using scanning electron microscopy (GeminiSEM 300). The elementary location of sulfur in nanofiber was scanned using energy-dispersive X-ray spectroscopy. Atomic force microscopy images were collected using a Bruker Dimension FastScan. X-ray Photoelectron Spectroscopy was conducted by Thermo Scientific Escalab 250Xi. X-ray diffraction patterns were collected using a Bruker D8 advance. Electrical properties and neuromorphic functions of the NAPPN were

measured using a PDA semiconductor analyzer under an ambient environment.

Data availability

The data that support the findings of this study are available from the corresponding author upon reasonable request.

Author contributions

Y. T. X.: conceptualization, methodology, visualization, formal analysis, data curation, writing – original draft, and writing – review & editing. D. P. L.: conceptualization, visualization, formal analysis, writing – original draft, and writing – review & editing. S. L. D.: validation and formal analysis. J. Y. Z.: data curation and validation. Z. Y. G.: data curation and formal analysis. X. L.: data curation and formal analysis. L. Z. X.: conceptualization, supervision, and funding acquisition. J. H.: conceptualization, funding acquisition, supervision, project administration, writing – original draft, and writing – review and editing.

Conflicts of interest

The authors declare no conflict of interest.

Acknowledgements

References

1 X. Deng, S. Q. Wang, Y. X. Liu, N. Zhong, Y. H. He, H. Peng, P. H. Xiang and C. G. Duan, *Adv. Funct. Mater.*, 2021, **31**, 2101099.

2 A. I. Basbaum, D. M. Bautista, G. Scherrer and D. Julius, *Cell*, 2009, **139**, 267–284.

3 C. Peirs and R. P. Seal, *Science*, 2016, **354**, 578–584.

4 I. M. Chiu, B. A. Heesters, N. Ghasemlou, C. A. Von Hehn, F. Zhao, J. Tran, B. Wainger, A. Strominger, S. Muralidharan, A. R. Horswill, J. B. Wardenburg, S. W. Hwang, M. C. Carroll and C. J. Woolf, *Nature*, 2013, **501**, 52–57.

5 J. H. Yoon, Z. Wang, K. M. Kim, H. Wu, V. Ravichandran, Q. Xia, C. S. Hwang and J. J. Yang, *Nat. Commun.*, 2018, **9**, 417.

6 R. Yu, Y. Yan, E. Li, X. Wu, X. Zhang, J. Chen, Y. Hu, H. Chen and T. Guo, *Mater. Horiz.*, 2021, **8**, 2797–2807.

7 X. Chen, B. Chen, B. Jiang, T. Gao, G. Shang, S.-T. Han, C.-C. Kuo, V. A. L. Roy and Y. Zhou, *Adv. Funct. Mater.*, 2023, **33**, 2208807.

8 H. Patil, H. Kim, K. D. Kadam, S. Rehman, S. A. Patil, J. Aziz, T. D. Dongale, Z. Ali Sheikh, M. Khalid Rahmani,

M. F. Khan and D.-K. Kim, *ACS Appl. Mater. Interfaces*, 2023, **15**, 13238–13248.

9 P. P. Patil, S. S. Kundale, S. V. Patil, S. S. Sutar, J. Bae, S. J. Kadam, K. V. More, P. B. Patil, R. K. Kamat, S. Lee and T. D. Dongale, *Small*, 2023, **19**, 2303862.

10 Y. Ren, J.-Q. Yang, L. Zhou, J.-Y. Mao, S.-R. Zhang, Y. Zhou and S.-T. Han, *Adv. Funct. Mater.*, 2018, **28**, 1870357.

11 Y. Ren, J.-Q. Yang, L. Zhou, J.-Y. Mao, S.-R. Zhang, Y. Zhou and S.-T. Han, *Adv. Funct. Mater.*, 2018, **28**, 1805599.

12 Y. Zhou, S. Han, G. Zhou, W.-Y. Wong and V. A. L. Roy, *Appl. Phys. Lett.*, 2013, **102**, 083301.

13 S. Ji, Q.-J. Sun, S. Venkatesh, Y. Yan, Y. Zhou, J. Zhuang, L. Zhou, S. Han, Z.-X. Xu and V. A. L. Roy, *Low-voltage extended gate organic thin film transistors for ion sensing based on semi-conducting polymer electrodes*, SPIE, 2016.

14 G. Liu, Q. Li, W. Shi, Y. Liu, K. Liu, X. Yang, M. Shao, A. Guo, X. Huang, F. Zhang, Z. Zhao, Y. Guo and Y. Liu, *Adv. Funct. Mater.*, 2022, **32**, 2200959.

15 H. Wei, Y. Ni, L. Sun, H. Yu, J. Gong, Y. Du, M. Ma, H. Han and W. Xu, *Nano Energy*, 2021, **81**, 105648.

16 M. Yang, X. Zhao, Q. Tang, N. Cui, Z. Wang, Y. Tong and Y. Liu, *Nanoscale*, 2018, **10**, 18135–18144.

17 X. Li, Y. Liu, J. Zhang, F. Wu, M. Hu and H. Yang, *Adv. Intell. Syst.*, 2022, **4**, 2200015.

18 S. Z. Bisri, S. Shimizu, M. Nakano and Y. Iwasa, *Adv. Mater.*, 2017, **29**, 1607054.

19 D. Wang, S. Zhao, R. Yin, L. Li, Z. Lou and G. Shen, *npj Flex. Electron.*, 2021, **5**, 13.

20 S. Dai, X. Liu, Y. Liu, Y. Xu, J. Zhang, Y. Wu, P. Cheng, L. Xiong and J. Huang, *Adv. Mater.*, 2023, **35**, 2300329.

21 S. Jiang, Y. He, R. Liu, C. Chen, L. Zhu, Y. Zhu, Y. Shi and Q. Wan, *IEEE Trans. Electron Devices*, 2021, **68**, 415–420.

22 F. Z. Li, H. R. Liu, J. M. Guo, X. Y. Zhou, K. K. Liu, L. Z. Liang, X. Y. Pei, F. C. Zhou, F. Huang, H. Wang and Y. H. Liu, *Adv. Intell. Syst.*, 2022, **4**, 2200233.

23 Y. Li, K. Yin, Y. Diao, M. Fang, J. Yang, J. Zhang, H. Cao, X. Liu and J. Jiang, *Nanoscale*, 2022, **14**, 2316–2326.

24 L. Wei, J. Jiang and Q. Wan, *Adv. Electron. Mater.*, 2022, **8**, 2101174.

25 G. Feng, J. Jiang, Y. Zhao, S. Wang, B. Liu, K. Yin, D. Niu, X. Li, Y. Chen, H. Duan, J. Yang, J. He, Y. Gao and Q. Wan, *Adv. Mater.*, 2020, **32**, e1906171.

26 X. Wang, Y. Yan, E. Li, Y. Liu, D. Lai, Z. Lin, Y. Liu, H. Chen and T. Guo, *Nano Energy*, 2020, **75**, 104952.

27 D. Hu, X. Wang, H. Chen and T. Guo, *Adv. Funct. Mater.*, 2017, **27**, 1703541.

28 H. Yang, Y. Liu, X. Wu, Y. Yan, X. Wang, S. Lan, G. Zhang, H. Chen and T. Guo, *Adv. Electron. Mater.*, 2019, **5**, 1900864.

29 Y. Bian, K. Liu, Y. Ran, Y. Li, Y. Gao, Z. Zhao, M. Shao, Y. Liu, J. Kuang, Z. Zhu, M. Qin, Z. Pan, M. Zhu, C. Wang, H. Chen, J. Li, X. Li, Y. Liu and Y. Guo, *Nat. Commun.*, 2022, **13**, 7163.

30 H. Wang, M. Yang, Q. Tang, X. Zhao, Y. Tong and Y. Liu, *Adv. Funct. Mater.*, 2019, **29**, 1901107.

31 W. A. Katz and R. Rothenberg, *J. Clin. Rheumatol.*, 2005, **11**, 11–15.

32 T. Hucho and J. D. Levine, *Neuron*, 2007, **55**, 365–376.

33 D. M. Bautista, J. Siemens, J. M. Glazer, P. R. Tsuruda, A. I. Basbaum, C. L. Stucky, S.-E. Jordt and D. Julius, *Nature*, 2007, **448**, 204–208.

34 M. S. Gold and G. F. Gebhart, *Nat. Med.*, 2010, **16**, 1248–1257.

35 P. Baral, S. Udit and I. M. Chiu, *Nat. Rev. Immunol.*, 2019, **19**, 433–447.

36 Y. Lee, J. Y. Oh, W. Xu, O. Kim, T. R. Kim, J. Kang, Y. Kim, D. Son, J. B. Tok, M. J. Park, Z. Bao and T. W. Lee, *Sci. Adv.*, 2018, **4**, eaat7387.

37 L. Liu, W. Xu, Y. Ni, Z. Xu, B. Cui, J. Liu, H. Wei and W. Xu, *ACS Nano*, 2022, **16**, 2282–2291.

38 M. K. Singh, A. Kumar and R. Prakash, *Mater. Sci. Eng., B*, 2017, **217**, 12–17.

39 K. Sim, F. Ershad, Y. Zhang, P. Yang, H. Shim, Z. Rao, Y. Lu, A. Thukral, A. Elgalad, Y. Xi, B. Tian, D. A. Taylor and C. Yu, *Nat. Electron.*, 2020, **3**, 775–784.

40 Y. S. Guan, A. Thukral, S. Zhang, K. Sim, X. Wang, Y. Zhang, F. Ershad, Z. Rao, F. Pan, P. Wang, J. Xiao and C. Yu, *Sci. Adv.*, 2020, **6**, eabb3656.

41 J. H. Kim, K. G. Cho, D. H. Cho, K. Hong and K. H. Lee, *Adv. Funct. Mater.*, 2021, **31**, 2010199.

42 C. J. Woolf and Q. Ma, *Neuron*, 2007, **55**, 353–364.

43 J. Zhang, Z. Guo, T. Sun, P. Guo, X. Liu, H. Gao, S. Dai, L. Xiong and J. Huang, *SmartMat*, 2023, **4**, e1246.

44 J. Zhang, P. Guo, Z. Guo, L. Li, T. Sun, D. Liu, L. Tian, G. Zu, L. Xiong and J. Zhang, *Adv. Funct. Mater.*, 2023, **33**, 2302885.

45 J. Zhang, Q. Shi, R. Wang, X. Zhang, L. Li, J. Zhang, L. Tian, L. Xiong and J. Huang, *InfoMat*, 2021, **3**, 904–916.

46 D. Hao, Z. Yang, J. Huang and F. Shan, *Adv. Funct. Mater.*, 2023, **33**, 2211467.

47 H. Chen, Y. Hou, Y. Shi, Y. Zhang, S. Wang, Q. Peng and H. Huang, *J. Am. Chem. Soc.*, 2023, **145**, 11988–11996.

48 T. Liu, Q. Lin, Y. Ma, S. Wang, H. Chen, Y. Wei, Y. Song, L. Shen, F. Huang and H. Huang, *Adv. Opt. Mater.*, 2022, **10**, 2201104.

49 S. Dai, Y. Zhao, Y. Wang, J. Zhang, L. Fang, S. Jin, Y. Shao and J. Huang, *Adv. Funct. Mater.*, 2019, **29**, 1903700.

50 J. Zhang, T. Sun, S. Zeng, D. Hao, B. Yang, S. Dai, D. Liu, L. Xiong, C. Zhao and J. Huang, *Nano Energy*, 2022, **95**, 106987.

51 X. Yan, L. Zhang, H. Chen, X. Li, J. Wang, Q. Liu, C. Lu, J. Chen, H. Wu and P. Zhou, *Adv. Funct. Mater.*, 2018, **28**, 1803728.

52 S. Wang, C. Chen, Z. Yu, Y. He, X. Chen, Q. Wan, Y. Shi, D. W. Zhang, H. Zhou, X. Wang and P. Zhou, *Adv. Mater.*, 2019, **31**, 1806227.

53 J. Zhang, Y. Lu, S. Dai, R. Wang, D. Hao, S. Zhang, L. Xiong and J. Huang, *Research*, 2021, **2021**, 7131895.

54 D. Liu, Q. Shi, S. Dai and J. Huang, *Small*, 2020, **16**, e1907472.

55 J. Zhu, Y. Yang, R. Jia, Z. Liang, W. Zhu, Z. U. Rehman, L. Bao, X. Zhang, Y. Cai, L. Song and R. Huang, *Adv. Mater.*, 2018, **30**, 1800195.

56 Z. Wu, P. Shi, R. Xing, T. Yu, L. Zhao, L. Wei, D. Wang, S. Yan, Y. Tian, L. Bai and Y. Chen, *Adv. Electron. Mater.*, 2022, **8**, 2200078.

57 C.-S. Yang, D.-S. Shang, N. Liu, E. J. Fuller, S. Agrawal, A. A. Talin, Y.-Q. Li, B.-G. Shen and Y. Sun, *Adv. Funct. Mater.*, 2018, **28**, 1804170.

58 W. D. Tracey, *Curr. Biol.*, 2017, **27**, 129–133.

59 S. Macedo-Júnior, F. Nascimento, M. Luiz-Cerutti and A. Santos, *Purinergic Signalling*, 2021, **17**, 303–312.

60 M. Toyota, D. Spencer, S. Sawai-Toyota, W. Jiaqi, T. Zhang, A. J. Koo, G. A. Howe and S. Gilroy, *Science*, 2018, **361**, 1112–1115.

61 J. Jiang, W. Hu, D. Xie, J. Yang, J. He, Y. Gao and Q. Wan, *Nanoscale*, 2019, **11**, 1360–1369.

62 V. Neugebauer and W. Li, *J. Neurophysiol.*, 2002, **87**, 103–112.

63 D. Dev, M. S. Shawkat, A. Krishnaprasad, Y. Jung and T. Roy, *IEEE Electron Device Lett.*, 2020, **41**, 1440–1443.

64 S. Ke, Y. He, L. Zhu, Z. Jiang, H. Mao, Y. Zhu, C. Wan and Q. Wan, *Adv. Electron. Mater.*, 2021, **7**, 2100487.

65 N. Temour'yants, A. Kostyuk and K. Tumanyants, *Neurophysiology*, 2011, **42**, 276–285.

66 C. Torsney, *Curr. Opin. Physiol.*, 2019, **11**, 51–57.

67 A. E. Dubin and A. Patapoutian, *J. Clin. Invest.*, 2010, **120**, 3760–3772.

68 P. Bessou and E. Perl, *J. Neurophysiol.*, 1969, **32**, 1025–1043.

69 D. Julius and A. I. Basbaum, *Nature*, 2001, **413**, 203–210.

70 Z. He, H. Shen, D. Ye, L. Xiang, W. Zhao, J. Ding, F. Zhang, C.-A. Di and D. Zhu, *Nat. Electron.*, 2021, **4**, 522–529.

71 Y. Zhao, G. Feng and J. Jiang, *Solid-State Electron.*, 2020, **165**, 107767.

72 L. J. Macpherson, A. E. Dubin, M. J. Evans, F. Marr, P. G. Schultz, B. F. Cravatt and A. Patapoutian, *Nature*, 2007, **445**, 541–545.

73 G. Feng, Y. Zhao and J. Jiang, *Solid-State Electron.*, 2019, **153**, 16–22.

74 Y. Kim, Y. J. Kwon, D. E. Kwon, K. J. Yoon, J. H. Yoon, S. Yoo, H. J. Kim, T. H. Park, J. W. Han and K. M. Kim, *Adv. Mater.*, 2018, **30**, 1704320.